metals

MDPI

Article

Stress Corrosion Cracking of Ultrafine-Grained Ti-2Fe-0.1B Alloying after Equal Channel Angular Pressing

Shuai Huang [1,2], Yutong Jin [1], Yu Wang [1], Yuecheng Dong [1,2,*], Hui Chang [1] and Igor V. Alexandrov [2,*]

[1] College of Materials Science and Engineering, Tech Institute for Advanced Materials, Nanjing Tech University, Nanjing 211816, China; shuaihuang2021@163.com (S.H.); 202261103003@njtech.edu.cn (Y.J.); 202121003004@njtech.edu.cn (Y.W.); ch2006@njtech.edu.cn (H.C.)

[2] Department of Materials Science and Physics of Metals, Ufa University of Science and Technology, Ufa 450008, Russia

* Correspondence: dongyuecheng@njtech.edu.cn (Y.D.); alexandrov.iv@ugatu.su (I.V.A.)

Abstract: In the present study, the stress corrosion cracking (SCC) of ultrafine-grained (UFG) Ti-2Fe-0.1B prepared by equal channel angular pressing (ECAP) was investigated by a slow strain rate test (SSRT) with in-site electrochemical equipment. In comparison with the atmosphere, results indicated that the mechanical properties of Ti-2Fe-0.1B alloy degraded in the simulated sea water, and the SCC sensitivity of UFG Ti-2Fe-0.1B alloy is much lower than the initial coarse-grained (CG) state. The enhanced SCC resistance of UFG Ti-2Fe-0.1B alloy could be attributed to the mechanical and corrosive aspects simultaneously. First of all, the strength of UFG Ti-2Fe-0.1B alloy is much higher than the CG state, but the elongation to failure of UFG Ti-2Fe-0.1B alloy decreased more than 1.8 times. The UFG sample suffered crack initiation until failure with a relative short time and low plastic deformation, which weakened the effect of corrosion during SSRT. In addition, X-ray photoelectron spectroscopy (XPS) revealed that the thickness of the passivation film of the UFG Ti-2Fe-0.1B alloy is thicker and that the component of the passivation film possesses a higher proportion of TiO_2 in the same etched depth, which is beneficial to the corrosion resistance. Furthermore, according to the in-site electrochemical experiment curves, it is believed that the passivation film has a higher repair ability after cracking during SSRT for the UFG Ti-2Fe-0.1B alloy due to the decrease in grain size and the increase in dislocation density.

Keywords: stress corrosion cracking; titanium alloy; ultrafine-grained; passivation film

check for updates

Citation: Huang, S.; Jin, Y.; Wang, Y.; Dong, Y.; Chang, H.; Alexandrov, I.V. Stress Corrosion Cracking of Ultrafine-Grained Ti-2Fe-0.1B Alloying after Equal Channel Angular Pressing. *Metals* **2023**, *13*, 1316. https://doi.org/10.3390/met13071316

Academic Editor: Davood Nakhaie

Received: 29 June 2023
Revised: 19 July 2023
Accepted: 21 July 2023
Published: 24 July 2023

Copyright: © 2023 by the authors. Licensee MDPI, Basel, Switzerland. This article is an open access article distributed under the terms and conditions of the Creative Commons Attribution (CC BY) license (https://creativecommons.org/licenses/by/4.0/).

1. Introduction

Severe plastic deformation (SPD) can effectively refine the microstructure to submicron or nanoscale by introducing large strains during the deformation process and then dramatically enhance the physical and chemical behaviors of materials, such as strength, fatigue resistance, bio-compatibility, and electrical conductivity [1–4]. Among them, equal channel angular pressing (ECAP) is one of the most promising methods, which is available to achieve bulk materials with uniform microstructure and can be processed continuously [5].

Titanium and its alloys have been widely used in fields such as petrochemical, aerospace, and marine engineering due to their unique specific strength, excellent corrosion resistance, high temperature resistance, and good compatibility [6–8]. In recent decades, the effect of grain size on corrosion resistance has been extensively studied and the conclusions are inconsistent. For instance, Maleki-Ghaleh [9] and Kim [10] found that ultrafine-grained (UFG) pure titanium processed by ECAP shows stronger corrosion resistance than coarse-grained (CG) state in simulated body fluid, HCl, and H_2SO_4 solutions. As a contrast, Nie [11] found that the corrosion resistance of UFG-Ti prepared by high pressure torsion (HPT) in a 3.5 wt% NaCl solution was lower than that of CG Ti. Garbacz [12] studied the corrosion performance of UFG-Ti prepared by hydrostatic extrusion (HE) in 0.15 mol/L NaCl solution by auger electron spectroscopy (AES) and Ar^+ sputtering

technology and found that the corrosion resistance of UFG-Ti decreased compared with CG-Ti. It is acceptable that the corrosion behavior of materials is affected by various internal and external factors, such as oxygen content, ion concentration, and pH value of the corrosive medium [13], as well as grain boundary, texture, and secondary phase of the microstructure [14–16].

It is well known that the excellent corrosion resistance of titanium alloy benefits from the dense oxide film formed spontaneously on its surface, which isolates the corrosion medium from the substrate [17]. However, the passivation film of titanium alloy is prone to cracking when it is subjected to stress in actual application. When the substrate is exposed to corrosive medium, corrosion occurs, making the titanium alloy lose its efficacy easier. The damage to specific materials under the combined action of stress and a specific corrosion medium is called stress corrosion cracking (SCC). Compared with numerous research on the corrosion behavior of titanium alloy, studies on the SCC behavior and fracture mechanism of titanium alloy are very limited. The SCC behavior is also affected intensively by corrosion medium and microstructure. Our group [18] found that the lamellar microstructure of TC4 ELI alloy exhibited significantly higher stress corrosion sensitivity than the equiaxed, which could be attributed to the higher α phase content and presence of triangular grain boundaries, which promoted an active anodic reaction and facilitated the formation of hydrides. Chi [19] proposed that lamellar α microstructure with different orientations and a large α colony can improve crack propagation resistance and reduce SCC in simulated oilfield brine. Liu [20] found that hydrostatic pressure also affects the adsorption and penetration of hydrogen, thus promoting the stress corrosion of titanium alloy. Joseph [21] investigated hot salt stress corrosion cracking in Ti6246 alloy, transgranular fracture, and the existence of hydride, which supported the suggestion that hydrogen charging leads to cracking in stress corrosion scenarios.

A novel low-cost Ti-2Fe-0.1B alloy was designed by our group that possesses good strength, ductility, hot deformation, and corrosion behavior [22–24]. Considering studies on the effect of grain size on stress corrosion of titanium alloys are still rare. In the present work, the stress corrosion behavior of UFG and CG Ti-2Fe-0.1B alloy in air and 3.5 wt% NaCl solution was investigated by a slow strain rate test (SSRT) at a strain rate of 1×10^{-6} s^{-1}, the open circuit potential (OCP) development of the sample was tested by in-situ electrochemical equipment, and the passive film of UFG and CG Ti-2Fe-0.1B alloy was analyzed by X-ray photoelectron spectroscopy (XPS).

2. Materials and Methods

The actual chemical composition of the Ti-2Fe-0.1B alloy is composed of 1.89% Fe, 0.08% B, 0.014% C, 0.0012% H, 0.062% O, 0.004% N, and the balance of Ti. The initial state of materials is melted into ingots with a diameter of about 420 mm by a consumable electrode melting furnace twice; the diameter of the ingot casting is 420 mm. The first forging process (cogging, upsetting, and drawing-out) made the diameter decrease to 300 mm at a temperature range of 1020–1050 °C. Then, the precision forging was performed at 900–950 °C to make the diameter of the sample decrease to 125 mm. The sample was finally machined to a diameter of 120 mm as a result of peeling. The subsequent rolling process was performed at 836 °C (the initial temperature) and adopted a 20-stand continuous rolling process. The rolling deformation goes through the alternating multi-pass rolling of horizontal and vertical mills. The sample was rolled into a bar with a diameter ranging from 120 mm to 20 mm gradually (hereafter in CG Ti-2Fe-0.1B). Then, the four ECAP passes were carried out by route Bc (the Bc method means that the sample is always rotated 90° in one direction for extrusion processing) at 400 °C (hereafter in UFG Ti-2Fe-0.1B).

The microstructural characteristics of CG Ti-2Fe-0.1B and UFG Ti-2Fe-0.1B were characterized by TEM. The sample was ground to a thickness of approximately 60 μm, then polished using an RL-I electrolytic twin-jet. The accelerating voltage was 20 KV, and the temperature range was −15 °C to 0 °C. Tian G2 60–300 (FEI., Hillsboro, OR, USA) was used for TEM characterization at an accelerated voltage of 300 KV.

A K-Alpha+ X-ray photoelectron spectrometer (THERMO SCIENTIFIC., Waltham, MA, USA) was used to analyze the element composition and content of the surface and depth directions of the passivation films of CG and UFG Ti-2Fe-0.1B and the binding energy of Ti2p were compared and calibrated by using the binding energy of C1s (284.8 eV).

The SSRT test was conducted in accordance with GB/T 15970.7-2000, "Corrosion Stress Corrosion Test of Metals and Alloys, Part 7: Slow Strain Rate Test". The SSRT sample was prepared using Wire Electrical Discharge Machining (WEDM), and the surface and side of the sample were polished to a finish of 2000 mesh using SiC sandpaper. Following this, the sample was ultrasonically cleaned with anhydrous ethanol for 5 min and then dried. A YYF-50 slow strain tensile testing machine(BAIROE., Shanghai, China) was used to carry out the SSRT at a strain rate of 1×10^{-6} s^{-1}. At least three samples were tested under identical experimental conditions. After failure, the broken sample was cleaned with de-ionized water and dried, then fractured, and its lateral surface was observed by a JSM-6510 scanning electron microscope (JEL., Tokyo, Japan) with an accelerated voltage of 15 KV.

SSRT was carried out in a 3.5 wt% NaCl solution (Lingfeng Chemical Reagent CO, Shanghai, China), and the OCP of the sample was monitored in real time with a CHI 660E electrochemical workstation (CH Instruments, Austin, TX, USA). A three-electrode system is adopted, in which the reference electrode (RE) is an Ag/AgCl electrode, the counter electrode (CE) is a platinum sheet, and the working electrode (WE) is a standard SSRT sample segment. Prior to experimentation, the samples were immersed in a 3.5 wt% NaCl solution for 24 h under a static tension of 350 N to ensure stable surface conditions.

3. Results

3.1. TEM Microstructural Characterization

Figure 1 shows TEM images of CG and UFG Ti-2Fe-0.1B, respectively. Obviously, the microstructure of CG Ti-2Fe-0.1B is mainly composed of dynamic recrystallization grains with equiaxed and dislocation-free grains; the grain boundaries are clear and less distorted. The microstructure of CG Ti-2Fe-0.1B comprises a large number of ultra-fine grains with grain sizes less than 1 μm and micro-grains with grain sizes around 10 μm; the average grain size is 1.72 μm. In contrast, the microstructure of UFG Ti-2Fe-0.1B alloy is mainly composed of dislocation cells and several subgrains; the microstructure is totally blurry due to a large number of dislocation tangles and dislocation piles; all the grains have high internal stress after suffering severe deformation; and the undistorted grains with clear grain boundaries and regular shapes are rarely seen. The microstructure of UFG Ti-2Fe-0.1B is more uniform, and the average grain size is 0.24 μm [22].

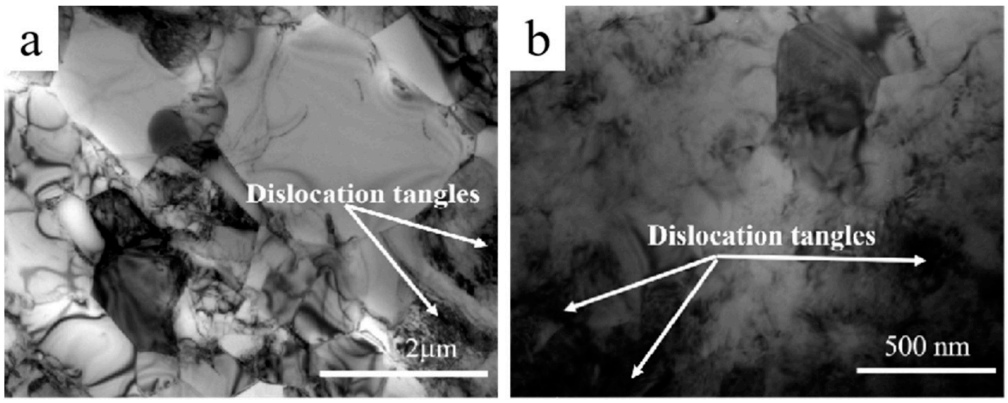


Figure 1. TEM micrographs of (**a**) CG Ti-2Fe-0.1B and (**b**) UFG Ti-2Fe-0.1B.

3.2. Mechanical Testing

Figure 2 presents the engineering stress-strain curves of CG and UFG Ti-2Fe-0.1B in air and a 3.5 wt% NaCl solution. In air, it can be seen that the CG Ti-2Fe-0.1B alloy has a good combination of strength and ductility, the yield strength and tensile strength reach 381 MPa and 625 MPa, respectively, while the elongation to failure remains at 28%, as indicated in Table 1. In particular, the CG Ti-2Fe-0.1B alloy shows a unique yield ratio, which can reach 0.6. Compared to the CG Ti-2Fe-0.1B alloy, after ECAP, the strength of the UFG Ti-2Fe-0.1B alloy increased dramatically; the yield strength and tensile strength reached 670 MPa and 834 MPa, respectively; the yield ratio increased to 0.8 and the elongation to failure decreased to 10%. However, when a tensile test was performed in a 3.5 wt% NaCl solution, the yield strength and tensile strength of the CG Ti-2Fe-0.1B alloy decreased to 360 MPa and 608 MPa, respectively, and at the same time, the elongation to failure also decreased to 25%. As a contrast, the strength and ductility of UFG Ti-2Fe-0.1B alloy changed a little in a 3.5 wt% NaCl solution. Therein, the yield strength and tensile strength decreased to 657 MPa and 806 MPa, respectively, and the elongation to failure remained at 10%.

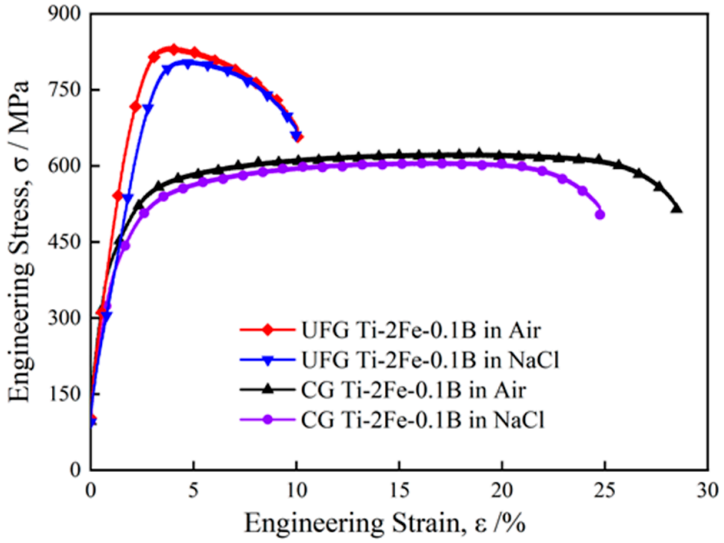


Figure 2. Engineering stress-strain curves of UFG Ti-2Fe-0.1B and CG Ti-2Fe-0.1B.

Table 1. Results of SCC testing in air and a 3.5 wt % NaCl solution.

Sample	$\sigma_{0.2}$/MPa	σ_b/MPa	A/%	$\sigma_{0.2}/\sigma_b$	I_{SSRT}
CG Ti-2Fe-0.1B in air	381 ± 5	629 ± 7	28 ± 1.2	0.6	0.0555
CG Ti-2Fe-0.1B in NaCl	360 ± 9	608 ± 10	25 ± 1.4	0.6	
UFG Ti-2Fe-0.1B in air	670 ± 4	834 ± 4	10 ± 0.7	0.8	0.0337
UFG Ti-2Fe-0.1B in NaCl	657 ± 6	807 ± 6	10 ± 0.9	0.8	

The decrease in strength and elongation shows that Ti-2Fe-0.1B has certain stress corrosion sensitivity in 3.5 wt% NaCl solution, and the stress corrosion sensitivity of materials can be measured by I_{SSRT} [25]:

$$I_{SSRT} = 1 - \frac{[R_{sol} \times (1 + A_{sol})]}{[R_{air} \times (1 + A_{air})]} \quad (1)$$

R_{sol} and A_{sol} represent tensile strength and elongation to failure in solution, respectively. R_{air} and A_{air} represent tensile strength and elongation to failure in air, respectively. This formula considers the variation of elongation to failure and tensile strength comprehensively. The higher the I_{SSRT} value, the greater the stress corrosion sensitivity. As indicated

in Table 1, both the CG and UFG Ti-2Fe-0.1B alloys have stress corrosion sensitivity, but the I_{SSRT} of UFG Ti-2Fe-0.1B decreased to 0.0337, which is much lower than that of the CG state. It can be concluded that the SCC behavior of UFG Ti-2Fe-0.1B is obviously optimized in comparison with the CG state.

3.3. Morphology of SCC

Figure 3 displays the fracture morphology of UFG and CG Ti-2Fe-0.1B in air and a 3.5 wt% NaCl solution, respectively. In air, the fracture morphology of CG Ti-2Fe-0.1B shows typical dimple rupture without any cleavage-like fracture characteristic. As can be seen in Figure 3a, the morphology features of dimples are deep and comparable homogeneous, which indicates a good ductility of CG Ti-2Fe-0.1B alloy [26]. However, the fracture morphology of CG Ti-2Fe-0.1B performed in a 3.5 wt% NaCl solution is relatively smooth (Figure 3b), and the morphology features of dimples are shallow and non-uniform. On the other hand, the UFG Ti-2Fe-0.1B alloy shows similar fracture morphology features both in air and in 3.5 wt% NaCl solution, although the dimples are much smaller than the CG state in the same corrosive medium.

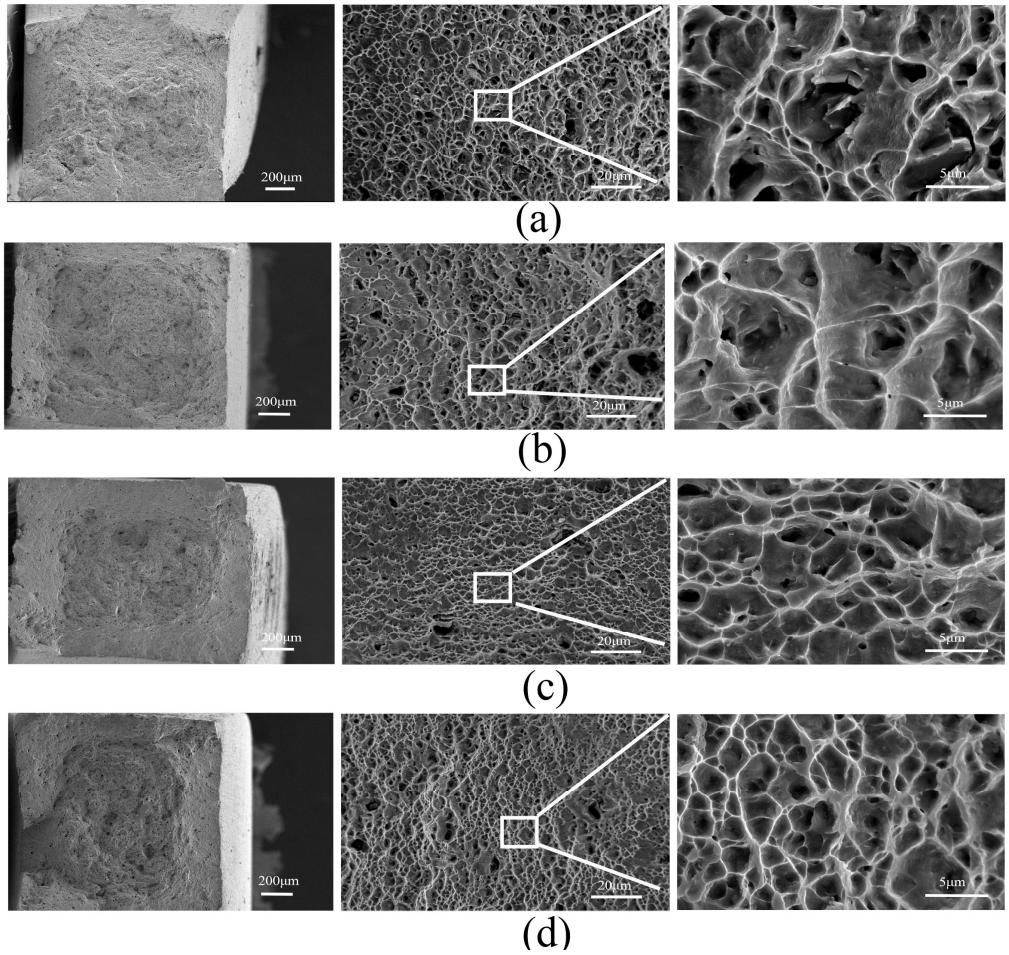


Figure 3. Fracture morphologies of CG (**a**,**b**) and UFG (**c**,**d**) Ti-Fe-B in air (**a**,**c**) and 3.5 wt% NaCl solution (**b**,**d**) after SSRT.

Figure 4 displays the fracture morphology of the lateral surfaces of CG and UFG Ti-2Fe-0.1B. Obviously, microcracks can be observed in the microstructure of all samples, but the morphology features are quite different. The microcracks of CG Ti-2Fe-0.1B show the form of holes with a diameter of 4 mm to 9 mm in air, while the microcracks spread laterally and become very long and narrow in a 3.5 wt% NaCl solution. On the other hand, the size of microcracks in UFG Ti-2Fe-0.1B is obviously smaller than that of CG

state; microcracks mostly exist in the form of long strips in the air conditioning, and the distribution is relatively uniform, but they tend to expand longitudinally in the 3.5 wt% NaCl solution.

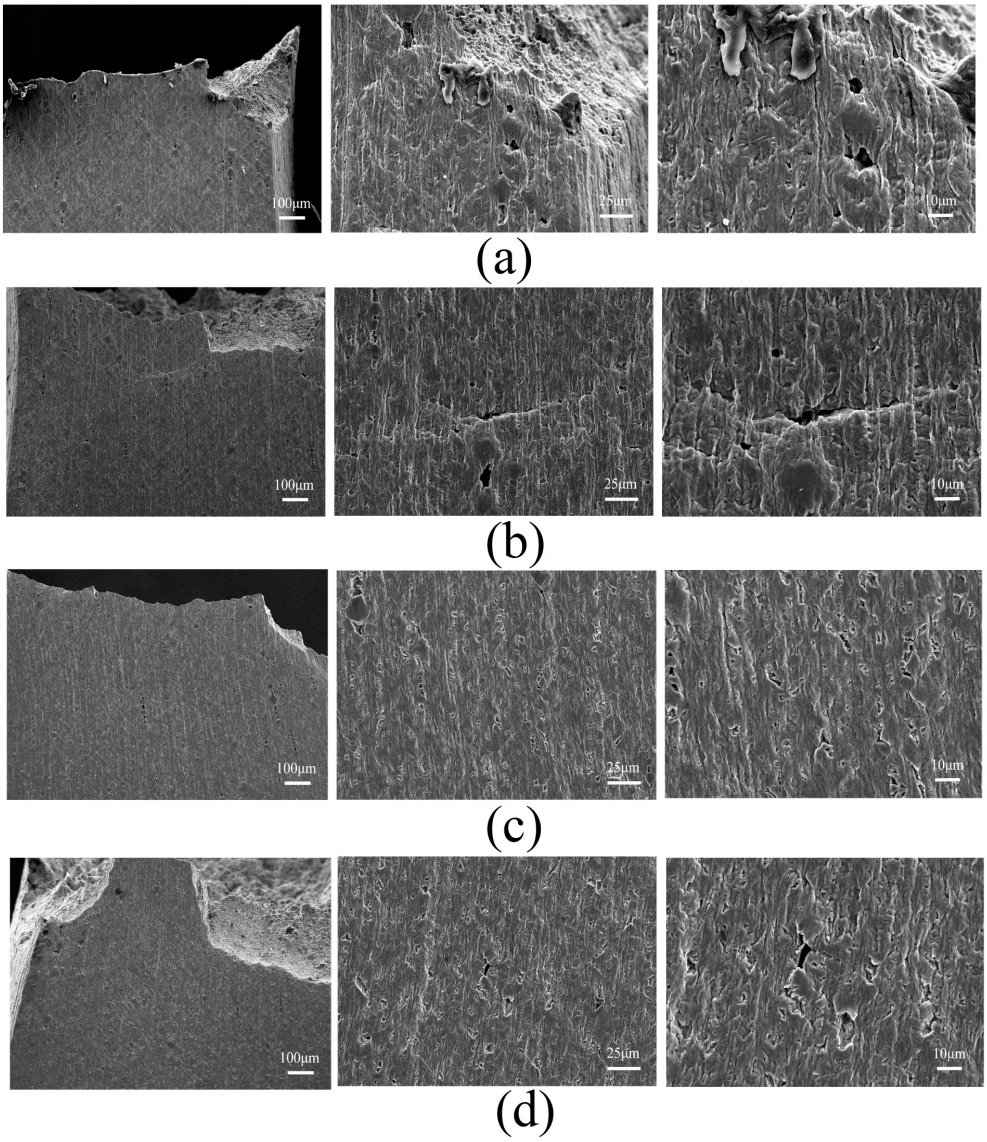


Figure 4. Lateral fracture morphologies of CG (**a**,**b**) and UFG (**c**,**d**) Ti-Fe-B in air (**a**,**c**) and 3.5 wt% NaCl solution (**b**,**d**) after SSRT.

3.4. In-Situ Open Circuit Potential Result

As is well known, when titanium alloys are immersed in solution without external stress, their OCP value fluctuates with the development of the surface state of the alloy and eventually approaches a stable state with a certain potential, which means the self-corrosion potential of the alloy in this environment [27]. It is interesting to observe the development of the OCP value of samples during SSRT. Hence, the transient changes in OCP of CG and UFG Ti-2Fe-0.1B alloys during SSRT in 3.5 wt% NaCl solution were obtained by in−situ electrochemical equipment, as indicated in Figure 5. During the initial stage of tensile stress, the OCP value of CG Ti-2Fe-0.1B first decreased from −1.11 V to −0.15 V, then slowly increased, and finally stabilized. In contrast, the OCP value of UFG Ti-2Fe-0.1B first experienced a brief fluctuation and increased from −0.09 V to −0.06 V, then decreased and frequently fluctuated in the range of −0.08 V to −0.11 V. On the whole period, the OCP curve of CG Ti-2Fe-0.1B is relatively smooth, while the OCP value of UFG Ti-2Fe-0.1B is

zigzag. More than that, the OCP values of Ti-2Fe-0.1B alloy are always higher than the CG state.

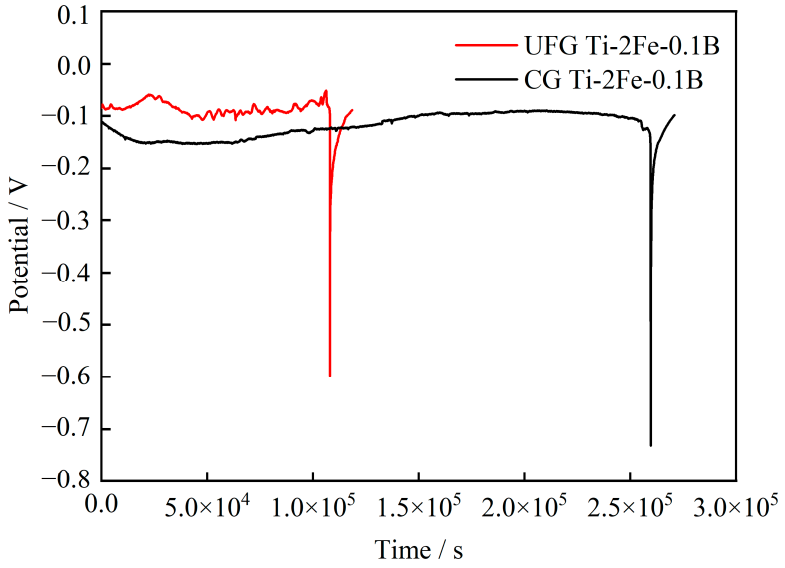


Figure 5. OCP transient changes of CG and UFG Ti-2Fe-0.1B in a 3.5 wt% NaCl solution.

3.5. Passivation Film Characterization

The elemental composition and content of passive films of CG and UFG Ti-2Fe-0.1B alloys were analyzed by XPS, and the Ti2p spectra were obtained after etching with different depths of 0 nm (surface), 2 nm, 4 nm, and 8 nm (Figure 6). On the surface, results indicated that the passive film of CG and UFG Ti-2Fe-0.1B alloys mainly consists of Ti^{4+}, Ti^{2+}, and Ti, which correspond to the ideal oxide TiO_2, suboxide TiO, and Ti, respectively. But the TiO_2 peak value of UFG Ti-2Fe-0.1B is much higher than that of the CG state. As the etching depth increased, the peak value of CG and UFG Ti-2Fe-0.1B alloy corresponding to Ti^{4+} decreased, while the peak value corresponding to low-valence titanium ions and Ti increased.

Table 2 shows the relative atomic concentration of titanium oxide as fitted by XPS. The relative concentration of TiO_2 in the passivation film of the CG Ti-2Fe-0.1B alloy is 54.3% on the surface, but for the UFG state, this value increased to 63.3%. With the increase in etching depth, the content of TiO_2 continuously decreased until it disappeared in 8 nm depth for both states; however, it is worthy to notice that the content of TiO_2 for UFG Ti-2Fe-0.1B alloy is higher than that of the CG state in the same etching depth. In particular, in the 4 nm depth, the content of TiO_2 for the UFG Ti-2Fe-0.1B alloy is more than 2 times that of the CG state.

Table 2. The concentration of titanium oxide at different depths.

Composition (%)	CG Ti-2Fe-0.1B				UFG Ti-2Fe-0.1B			
	Surface	2 nm	4 nm	8 nm	Surface	2 nm	4 nm	8 nm
TiO_2	54.3	36.5	13.4	0	63.3	46.8	28.3	0
Ti_2O_3	0	25.7	36.8	30.5	0	21.4	26.6	36.2
TiO	30.5	17.3	19.5	36.1	24.2	13.2	18.6	34.5
Ti	15.2	20.5	30.3	33.4	12.5	18.6	26.5	29.3

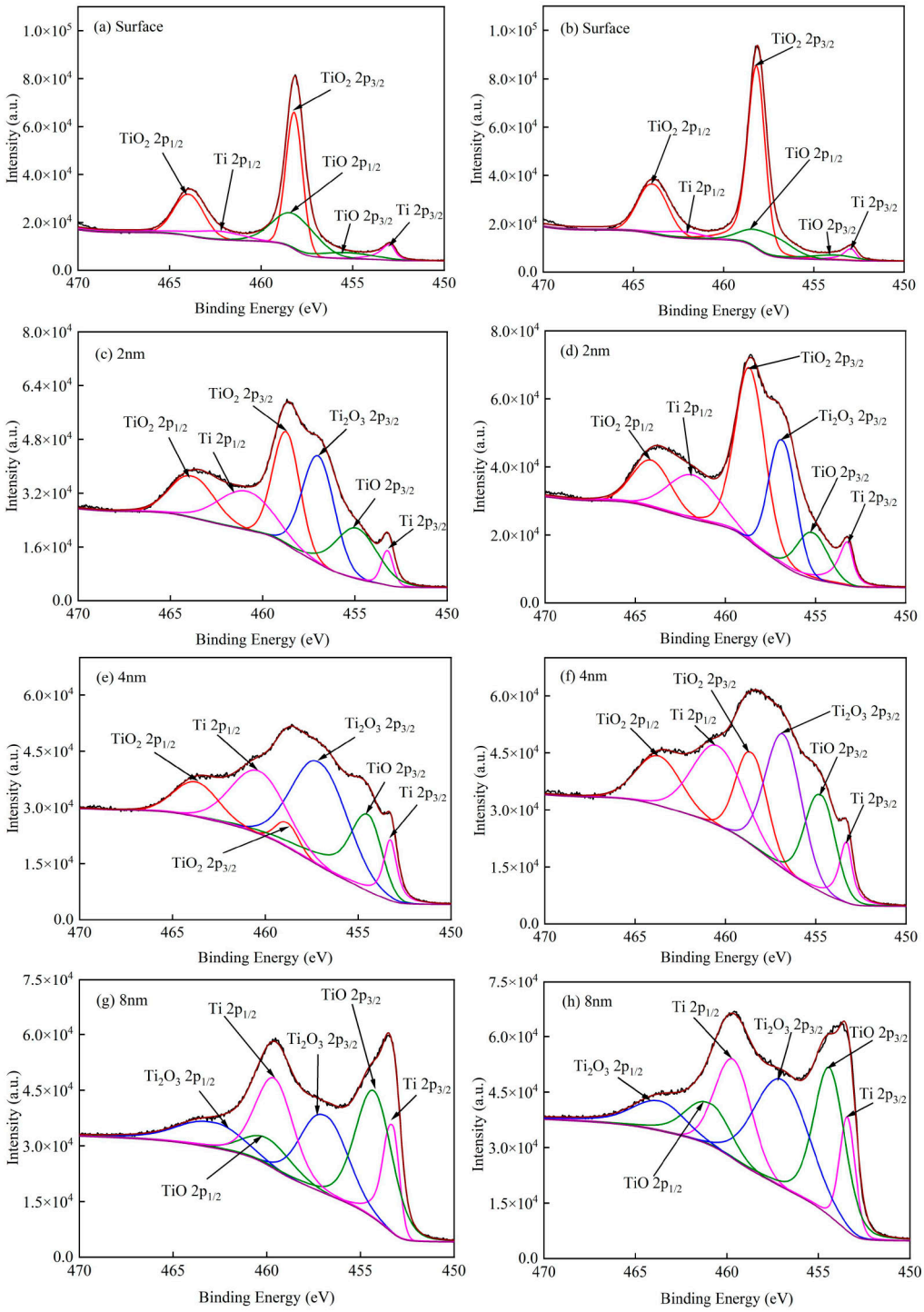


Figure 6. Ti2p XPS spectra of the passive film formed on (**a**,**c**,**e**,**g**) CG Ti-2Fe-0.1B and (**b**,**d**,**f**,**h**) UFG Ti-2Fe-0.1B in different depths.

4. Discussion

It is well known that the SCC of material is a result of the mutual effects of corrosion and mechanical factors. When the passivation film is cracked due to tensile stress, the fresh substrate is exposed to the solution medium, and the damaged metal surface becomes the anode, while the undamaged surface becomes the cathode. One of the SCC mechanisms is generally considered to be related to anodic dissolution [28]. The anode metal atoms are constantly dissolved, and because the anode area is small, the current density of the anode

will be large, which will lead to further corrosion of the fresh substrate. In this process, the following reactions occurred [29,30]:

$$Ti \rightarrow Ti^{3+} + 3e^{-} \quad (2)$$

$$Ti + 2H_2O \rightarrow TiO_2 + 4H^{+} + 4e^{-} \quad (3)$$

$$H^{+} + e^{-} \rightarrow H \quad (4)$$

$$Ti^{3+} + H_2O \rightarrow TiO^{2+} + 2H^{+} + e^{-} \quad (5)$$

In the oxygen-enriched environment, the damaged passive film of the sample could sometimes be repaired by re-passivation, although the position where metastable point corrosion occurred is weaker than the normal position of the passive film [31]. In addition, the re-passivation film will rupture again under the action of tensile stress. Finally, under the combined effect of corrosion and tensile stress, cracks gradually formed at the corrosion damage site and continued to expand until the material failed.

Meanwhile, the process of anodic dissolution is always accompanied by the generation of hydrogen ions. When hydrogen is enriched, it could promote the formation and movement of dislocations, and the energy threshold required for fracture at stress concentrations in titanium alloys is reduced [32,33].

As mentioned above, after ECAP, the UFG Ti-2Fe-0.1B alloy possesses lower stress corrosion sensitivity than that of the CG state, which means better SCC resistance. It can be explained from two angles. From the corrosion aspect, it is well known that Fe is a β-stabilizing element, which has a low solubility in alpha-Ti and mainly dissolves in beta-Ti. On the other side, the B element does not dissolve in titanium alloy and always presents in the microstructure as TiB particles. Both Fe and B element additions can benefit the refinement of ingot structure; meanwhile, the reduction in grain size of Ti-2Fe-0.1B alloy by ECAP can effectively improve the segregation of elements and weaken the galvanic effect [34,35]. Our group [22] characterized the surface morphology of CG and UFG Ti-2Fe-0.1B after potentiodynamic scanning by SEM, and it was found that the corrosion pit volume produced by selective dissolution due to the galvanic effect in CG Ti-2Fe-0.1B was significantly higher than that in UFG Ti-2Fe-0.1B. This result proves that in UFG Ti-2Fe-0.1B, the distribution of alloying elements in the α and β phases is more uniform and the microstructure is more homogeneous, which could reduce the risk of pitting corrosion when the fresh substrate is exposed to corrosive medium because the passivation film ruptures under the influence of external tensile stress. Otherwise, stress concentration will easily occur at the position where pitting corrosion occurs under the action of tensile stress, which will promote the occurrence of cracking. On the other hand, the self-repairing capability of passivation film could be improved due to the refinement of grain size. As shown in Figure 5, the OCP curve of CG Ti-2Fe-0.1B decreases at the beginning of imposed tensile stress because the passivation films formed on titanium and titanium alloys have a double-layer structure [36]. According to the corrosion principle of passivation metals, the loose outer layer of the film is transformed into a dense inner layer in aqueous solution [37]. When high Cl-irons are adsorbed by titanium alloys in NaCl solution, autocatalysis occurs and leads to the generation of new vacancies [38]. Meanwhile, due to local electrical neutrality, the newly generated oxygen vacancies significantly inhibit the transformation of stable Ti^{4+} from Ti^{3+} and Ti^{2+}, thus preventing the repair of the passive film. For the UFG Ti-2Fe-0.1B alloy, it also suffers the above process when it is subjected to tensile stress in a 3.5 wt% NaCl solution. At the beginning of deformation during SSRT, the OCP value also showed a downward trend. However, accompanied by the grain refinement of Ti-2Fe-0.1B during ECAP, a large number of grain boundaries and dislocations were introduced, which can provide more positions for the nucleation of passivation film, enhance passivation kinetics, and promote the faster formation of oxide film [39,40], so the OCP values recovered quickly. That is why the OCP curves of UFG Ti-2Fe-0.1B alloy show a zigzag wave. As

shown in Table 2, at the same etching depth, the relative concentration of TiO_2 in UFG Ti-2Fe-0.1B is always higher than that in the CG state. This result also proves that Ti^{3+} and Ti^{2+} in UFG Ti-2Fe-0.1B after grain refinement can be easily transformed into stable Ti^{4+}.

From the mechanical aspect, Wang et al. [41] found that the diffusivity of point defects (D_0) increased with increasing plastic deformation during SSRT. A higher D_0 value can increase the risk of pitting corrosion, as a higher vacancy density has a higher affinity for chloride ions, which can produce more pitting nucleation sites [42]. This means that in CG Ti-2Fe-0.1B, which has low strength but high plastic deformation ability due to dynamic recrystallized grain, metal vacancies are easier generated at the passivation film/solution interface and constantly migrate to the metal/passivation film interface, consuming metal atoms in the matrix. Oxygen vacancies and metal ions are generated at the interface of metal/passivation film, which migrate to the interface of passivation film/solution, and the oxides on the surface are constantly dissolved. As a result, the passive film is ruptured, which leads to corrosion pits and microcracks, which further become the origin of fracture, as shown in Figure 4b. However, Grain refinement increases the yield strength and tensile strength of UFG Ti-2Fe-0.1B dramatically, as shown in Figure 2. This greatly increases its ability to resist plastic deformation, which means fewer point vacancies could be generated for the UFG state during plastic deformation in a 3.5 wt% NaCl solution, which then inhibits the origination and propagation of pitting corrosion. It is worth noting that the above-mentioned point defects caused by SSRT in corrosive media are different from those introduced in the ECAP process. The defects introduced in the ECAP process, such as grain refinement and grain boundary slip, led to more grain boundaries; oxide protrusions can be embedded in high-density grain boundaries, increasing the interfacial adhesion between the Ti matrix and passivation film [43]. This not only improves the strength of the material but also makes the rupture of the passivation film more difficult under the action of tensile stress.

Finally, Compared to the UFG Ti-2Fe-0.1B alloy, the sample of CG Ti-2Fe-0.1B alloy took a relative long time to immerse in NaCl solution until it fractured because of its good ductility. As indicated in Figure 5, which implies that the effect of corrosion could play an important role in the whole process of failure. As a contrast, the UFG sample suffered crack initiation until failure in a relatively short time, which weakened the effect of corrosion during SSRT.

5. Conclusions

The SCC behavior of UFG Ti-2Fe-0.1B alloy processed by ECAP was studied by SSRT experiment with in situ electrochemical equipment; the passive film was analyzed by the XPS method; and the fracture morphology after fracture was observed by SEM. It can be concluded that:

(1) Both UFG and CG Ti-2Fe-0.1B alloys show certain stress-corrosion sensitivity. However, the stress corrosion sensitivity of UFG Ti-2Fe-0.1B processed by ECAP is much lower than that of CG Ti-2Fe-0.1B; the ISSRT value decreased from 0.0555 to 0.0337;
(2) Refinement of grain size and increase in dislocation density in UFG Ti-2Fe-0.1B can provide more sites for the nucleation of the passivation film, which enhances the passivation kinetics and increases the TiO_2 content and re-passivation ability of the passivation film;
(3) The UFG sample possesses high strength but low ductility; it took a relative short time and low plastic deformation from crack initiation until failure, which weakened the effect of corrosion during SSRT.

Author Contributions: S.H.: Methodology, Investigation, Validation, Formal analysis, Writing—original draft, Visualization. Y.J.: Data curation, Resources, Validation, Writing—review and editing. Y.W.: Data curation, Resources, Validation, Writing—review and editing. Y.D.: Conceptualization, Resources, Supervision, Funding acquisition, Writing—review and editing. H.C.: Conceptualization, Resources, Supervision, I.V.A.: Validation, Writing—review and editing, Funding acquisition. All authors have read and agreed to the published version of the manuscript.

Funding: This research was funded by National Key R&D Program of China (No. 2021YFB3700802), the National Natural Science Foundation of China (No. 51931008), Russian Science Foundation (No. 23-43-00041), and A Project Funded by the Priority Academic Program Development of Jiangsu Higher Education Institutions (PAPD).

Data Availability Statement: Not applicable.

Acknowledgments: The research is supported by the National Key R&D Program of China (No. 2021YFB3700802), the National Natural Science Foundation of China (No. 51931008), Russian Science Foundation (No. 23-43-00041), and A Project Funded by the Priority Academic Program Development of Jiangsu Higher Education Institutions (PAPD). The authors are grateful to the personnel of the Research Equipment Sharing Center "Nanotech" of Ufa University of Science and Technology for their assistance with instrumental analysis.

Conflicts of Interest: All authors declare that they have no conflict of interest.

References

1. Qarni, M.J.; Sivaswamy, G.; Rosochowski, A.; Boczkal, S. Effect of incremental equal channel angular pressing (I-ECAP) on the microstructural characteristics and mechanical behaviour of commercially pure titanium. *Mater. Des.* **2017**, *122*, 385–402. [CrossRef]
2. Sajadifar, S.V.; Yapici, G.; Demler, E.; Krooß, P.; Wegener, T.; Maier, H.; Niendorf, T. Cyclic deformation response of ultra-fine grained titanium at elevated temperatures. *Int. J. Fatigue* **2019**, *122*, 228–239. [CrossRef]
3. Claudia, G.-M.; Ivan, G.; Laia, O.-M.; Emilio, J.-P.; Maria-Pau, G.; Maurizio, V.; Luís, C.J.; Marta, P. Influence of ECAP process on mechanical, corrosion and bacterial properties of Zn-2Ag alloy for wound closure devices. *Mater. Des.* **2023**, *228*, 111817. [CrossRef]
4. Dalan, F.C.; de Lima Andreani, G.F.; Travessa, D.N.; Faizov, I.A.; Faizova, S.; Cardoso, K.R. Effect of ECAP processing on distribution of second phase particles, hardness and electrical conductivity of Cu-0.81 Cr-0.07 Zr alloy. *Trans. Nonferrous Met. Soc. China* **2022**, *32*, 217–232. [CrossRef]
5. Duan, Y.; Tang, L.; Xu, G.; Deng, Y.; Yin, Z. Microstructure and mechanical properties of 7005 aluminum alloy processed by room temperature ECAP and subsequent annealing. *J. Alloys Compd.* **2016**, *664*, 518–529. [CrossRef]
6. Banerjee, D.; Williams, J. Perspectives on titanium science and technology. *Acta Mater.* **2013**, *61*, 844–879. [CrossRef]
7. Pang, J.; Blackwood, D.J. Corrosion of titanium alloys in high temperature near anaerobic seawater. *Corros. Sci.* **2016**, *105*, 17–24. [CrossRef]
8. Yu, Z.; Dong, Y.; Li, X.; Niu, J.; Alexandrov, I.; Chang, H. Study on corrosion behavior of ultrafine-grained Ti-6Al-7Nb fabricated by equal channel angular pressing. *Metals* **2020**, *10*, 950. [CrossRef]
9. Maleki-Ghaleh, H.; Hajizadeh, K.; Hadjizadeh, A.; Shakeri, M.; Alamdari, S.G.; Masoudfar, S.; Aghaie, E.; Javidi, M.; Zdunek, J.; Kurzydlowski, K. Electrochemical and cellular behavior of ultrafine-grained titanium in vitro. *Mater. Sci. Eng. C* **2014**, *39*, 299–304. [CrossRef]
10. Kim, H.S.; Yoo, S.J.; Ahn, J.W.; Kim, D.H.; Kim, W.J. Ultrafine grained titanium sheets with high strength and high corrosion resistance. *Mater. Sci. Eng. A* **2011**, *528*, 8479–8485. [CrossRef]
11. Nie, M.; Wang, C.T.; Qu, M.; Gao, N.; Wharton, J.A.; Langdon, T.G. The corrosion behaviour of commercial purity titanium processed by high-pressure torsion. *J. Mater. Sci.* **2014**, *49*, 2824–2831. [CrossRef]
12. Garbacz, H.; Pisarek, M.; Kurzydłowski, K. Corrosion resistance of nanostructured titanium. *Biomol. Eng.* **2007**, *24*, 559–563. [CrossRef] [PubMed]
13. Balyanov, A.; Kutnyakova, J.; Amirkhanova, N.; Stolyarov, V.; Valiev, R.; Liao, X.; Zhao, Y.; Jiang, Y.; Xu, H.; Lowe, T. Corrosion resistance of ultra fine-grained Ti. *Scr. Mater.* **2004**, *51*, 225–229. [CrossRef]
14. Hoseini, M.; Shahryari, A.; Omanovic, S.; Szpunar, J.A. Comparative effect of grain size and texture on the corrosion behaviour of commercially pure titanium processed by equal channel angular pressing. *Corros. Sci.* **2009**, *51*, 3064–3067. [CrossRef]
15. Gurao, N.; Manivasagam, G.; Govindaraj, P.; Asokamani, R.; Suwas, S. Effect of texture and grain size on bio-corrosion response of ultrafine-grained titanium. *Metall. Mater. Trans. A* **2013**, *44*, 5602–5610. [CrossRef]
16. Li, X.; Dong, Y.; Dan, Z.; Chang, H.; Fang, Z.; Guo, Y. Corrosion behavior of ultrafine grained pure Ti processed by equal channel angular pressing. *Acta Metall. Sin.* **2019**, *55*, 967–975.
17. Ren, S.; Du, C.; Liu, Z.; Li, X.; Xiong, J.; Li, S. Effect of fluoride ions on corrosion behaviour of commercial pure titanium in artificial seawater environment. *Appl. Surf. Sci.* **2020**, *506*, 144759. [CrossRef]
18. Dong, Y.; Huang, S.; Wang, Y.; Zhang, B.; Alexandrov, I.; Chang, H.; Dan, Z.; Ma, L.; Zhou, L. Stress corrosion cracking of TC4 ELI alloy with different microstructure in 3.5% NaCl solution. *Mater. Charact.* **2022**, *194*, 112357. [CrossRef]
19. Chi, G.; Jiang, B.; Yi, D.; Yang, L.; Pan, S.; Liu, H.; Feng, C.; Mao, W. Effect of lamellar α on the stress corrosion cracking of Ti-6Al-4 V alloy in simulated oilfield brine. *Mater. Charact.* **2021**, *174*, 111000. [CrossRef]
20. Liu, R.; Xie, Y.; Jin, Y.; Cui, Y.; Liu, L.; Wang, F. Stress corrosion cracking of the titanium alloys under hydrostatic pressure resulting from the degradation of passive films. *Acta Mater.* **2023**, *252*, 118946. [CrossRef]

21. Joseph, S.; Lindley, T.C.; Dye, D.; Saunders, E.A. The mechanisms of hot salt stress corrosion cracking in titanium alloy Ti-6Al-2Sn-4Zr-6Mo. *Corros. Sci.* **2018**, *134*, 169–178. [CrossRef]
22. Wang, Y.; Li, X.; Alexandrov, I.; Ma, L.; Dong, Y.; Valiev, R.; Chang, H.; Zhang, B.; Wang, Y.; Zhou, L. Impact of equal channel angular pressing on mechanical behavior and corrosion resistance of hot-rolled Ti-2Fe-0.1 B alloy. *Materials* **2020**, *13*, 5117. [CrossRef] [PubMed]
23. Niu, J.; Dai, G.; Guo, Y.; Sun, Z.; Dan, Z.; Dong, Y.; Chang, H.; Alexandrov, I.V.; Zhou, L. Microstructure and mechanical properties of B modified Ti–Fe alloy manufactured by casting, forging and laser melting deposition. *Compos. Part B Eng.* **2021**, *216*, 108854. [CrossRef]
24. Zhang, B.; Wang, Y.; Chang, H.; Alexandrov, I.; Sun, Z.; Dong, Y.; Valiev, R.; Wang, Y.; Zhou, L. Effect of hydrogen on microstructure evolution and deformation behaviors of Ti-2Fe-0.1 B alloy. *J. Alloys Compd.* **2022**, *900*, 163473. [CrossRef]
25. *HB7235-1995*; Standard Practice for Slow Strain Rate Testing to Evaluate Stress Corrosion Cracking Susceptibility. Aviation Industry Corporation of China: Beijing, China, 1995.
26. Ren, L.; Xiao, W.; Chang, H.; Zhao, Y.; Ma, C.; Zhou, L. Microstructural tailoring and mechanical properties of a multi-alloyed near β titanium alloy Ti-5321 with various heat treatment. *Mater. Sci. Eng. A* **2018**, *711*, 553–561. [CrossRef]
27. Bai, Y.; Gai, X.; Li, S.; Zhang, L.-C.; Liu, Y.; Hao, Y.; Zhang, X.; Yang, R.; Gao, Y. Improved corrosion behaviour of electron beam melted Ti-6Al–4V alloy in phosphate buffered saline. *Corros. Sci.* **2017**, *123*, 289–296. [CrossRef]
28. Nguyen, T.T.; Bolivar, J.; Shi, Y.; Réthoré, J.; King, A.; Fregonese, M.; Adrien, J.; Buffiere, J.Y.; Baietto, M.C. A phase field method for modeling anodic dissolution induced stress corrosion crack propagation. *Corros. Sci.* **2018**, *132*, 146–160. [CrossRef]
29. Shi, Y.; Joseph, S.; Saunders, E.A.; Sandala, R.S.; Walker, A.; Lindley, T.C.; Dye, D. AgCl-induced hot salt stress corrosion cracking in a titanium alloy. *Corros. Sci.* **2021**, *187*, 109497. [CrossRef]
30. Joseph, S.; Kontis, P.; Chang, Y.; Shi, Y.; Raabe, D.; Gault, B.; Dye, D. A cracking oxygen story: A new view of stress corrosion cracking in titanium alloys. *Acta Mater.* **2022**, *227*, 117687. [CrossRef]
31. Cui, Y.-W.; Chen, L.-Y.; Liu, X.-X. Pitting corrosion of biomedical titanium and titanium alloys: A brief review. *Curr. Nanosci.* **2021**, *17*, 241–256. [CrossRef]
32. Wang, C.M.; Zhang, L.J.; Ma, Y.J.; Zhang, S.Z.; Yang, R.; Hu, Q.M. Hydrogen-surface interaction from first-principles calculations and its implication to hydrogen embrittlement mechanisms of titanium. *Appl. Surf. Sci.* **2023**, *621*, 156871. [CrossRef]
33. Gong, P.; Nutter, J.; Rivera-Diaz-Del-Castillo, P.; Rainforth, W. Hydrogen embrittlement through the formation of low-energy dislocation nanostructures in nanoprecipitation-strengthened steels. *Sci. Adv.* **2020**, *6*, eabb6152. [CrossRef]
34. Danoix, F.; Hoummada, K.; Maugis, P.; Rolland, N.; Debreux, C.; Blavette, D. Grain size effect on interfacial segregation in nanomaterials. *J. Phys. Chem. Solids* **2022**, *164*, 110620. [CrossRef]
35. Palumbo, G.; Erb, U. Enhancing the operating life and performance of lead-acid batteries via grain-boundary engineering. *mRS Bull.* **1999**, *24*, 27–32. [CrossRef]
36. Li, Z.; Wang, J.; Dong, Y.; Xu, D.; Zhang, X.; Wu, J.; Gu, T.; Wang, F. Synergistic effect of chloride ion and Shewanella algae accelerates the corrosion of Ti-6Al-4V alloy. *J. Mater. Sci. Technol.* **2021**, *71*, 177–185. [CrossRef]
37. Chen, L.Y.; Shen, P.; Zhang, L.; Lu, S.; Chai, L.; Yang, Z.; Zhang, L.C. Corrosion behavior of non-equilibrium Zr-Sn-Nb-Fe-Cu-O alloys in high-temperature 0.01 M LiOH aqueous solution and degradation of the surface oxide films. *Corros. Sci.* **2018**, *136*, 221–230. [CrossRef]
38. Qin, T.; Lin, X.; Yu, J.; Wang, M.; Guo, P.; Li, J.; Zhang, Y.; Liu, J.; Zhang, S.; Huang, W. Performance of different microstructure on electrochemical behaviors of laser solid formed Ti-6Al-4V alloy in NaCl solution. *Corros. Sci.* **2021**, *185*, 109392. [CrossRef]
39. Gu, Y.; Ma, A.; Jiang, J.; Li, H.; Song, D.; Wu, H.; Yuan, Y. Simultaneously improving mechanical properties and corrosion resistance of pure Ti by continuous ECAP plus short-duration annealing. *Mater. Charact.* **2018**, *138*, 38–47. [CrossRef]
40. Argade, G.; Panigrahi, S.; Mishra, R. Effects of grain size on the corrosion resistance of wrought magnesium alloys containing neodymium. *Corros. Sci.* **2012**, *58*, 145–151. [CrossRef]
41. Wang, J.; Song, S.; Li, D. Diffusivity of a point defect in the passive film on Ti with plastic deformation in 3.5% NaCl solution. *Thin Solid Film.* **2022**, *754*, 139304. [CrossRef]
42. Macdonald, D.D. The history of the point defect model for the passive state: A brief review of film growth aspects. *Electrochim. Acta* **2011**, *56*, 1761–1772. [CrossRef]
43. Balakrishnan, A.; Lee, B.; Kim, T.; Panigrahi, B. Corrosion behaviour of ultra fine grained titanium in simulated body fluid for implant application. *Trends Biomater. Artif. Organs* **2008**, *22*, 58–64.

Disclaimer/Publisher's Note: The statements, opinions and data contained in all publications are solely those of the individual author(s) and contributor(s) and not of MDPI and/or the editor(s). MDPI and/or the editor(s) disclaim responsibility for any injury to people or property resulting from any ideas, methods, instructions or products referred to in the content.